Modeling and Control of Variable Speed Wind Turbine Generators for Frequency Regulation

Mohammad Hasan Ravanji, Claudio A. Cañizares, *Fellow, IEEE*, and Mostafa Parniani, *Senior Member, IEEE*

***Abstract*— Wind turbine generators (WTG) can participate in system frequency regulation via virtual inertial controllers (VIC). In the presence of frequency disturbances, VIC temporarily regulates the WTG power output forcing it to release/absorb kinetic energy into/from the grid. With increasing penetration of WTGs in power systems, grid operators require these generators to provide frequency regulation services; however, kinetic energy release/absorption can destabilize WTGs. Hence, to address these issues, a new large-perturbation nonlinear WTG model is proposed in this paper, based on the WTG internal response that is used to tune typical VICs. Novel worst-case and optimal VIC tuning approaches are also proposed and discussed, based on the developed WTG nonlinear model. Several simulations are presented to test and validate the proposed model and VIC tuning techniques, demonstrating their adequate performance and advantages.**

***Index Terms*— Frequency regulation, frequency stability, virtual inertial controller, wind turbine generator, wind turbine modeling.**

I. Introduction

Frequency stability is “the ability of a power system to maintain steady frequency following a severe system upset resulting in a significant imbalance between generation and load” [1]. In order to guarantee frequency stability, grid operators employ hierarchical frequency controls, including inertial response and primary, secondary, and tertiary control levels. This paper mainly focuses on the inertial response and the primary frequency control of the system, in which, whenever a frequency disturbance (FD) occurs, a certain number of synchronous generators temporarily release/absorb kinetic energy into/from the grid to regulate the system frequency; hence, the more the synchronous generator inertia, the less the frequency excursions.

Fast-growing renewable generation, and in particular variable speed wind turbine generators (WTGs), do not typically provide inertial response, since their built-in high speed power electronic converters are controlled to extract the maximum power, and thus do not respond to system frequency variations [2], [3]; therefore, as the grid penetration of renewable generation increases, the overall system inertia is reduced. Consequently, FDs result in increased frequency change rates and nadirs, which may lead to frequency relays unwantedly tripping generators and loads [4]. However, WTGs inherently have the potential for inertial response [5]; thus, several researchers have focused on emulating inertial response with these generators to allow temporary energy release/absorption [5]–[13], using an essentially different approach than WTG deloading and droop control, as suggested for example in [14]. In these papers, virtual inertia is provided by short-term variations on the WTG electrical power set points whenever an FD occurs, using a derivative controller in [10], [13]; proportional-based controllers in [8] and [11]; combinations of the previous controllers in [4], [5], [7], and [9]; and heuristic nonlinear controllers in [12]. In general, derivate controllers mainly emulate inertial response, and proportional-based controllers play the role of temporary droop controllers, thus also increasing the system damping. None of these papers have investigated the WTGs internal response to FDs, assuming that the WTG penetration is not significant and that their internal stability is not an issue.

In the current paper, it is shown that the WTG internal stability is not guaranteed in systems with high renewable generation penetration. In this case, the role of the WTGs in system frequency stability is significant, requiring the release/absorption of energy from these sources when an FD occurs in the system. However, the more energy released, the less the WTG rotor speed; if the rotor speed reaches its minimum limit during a frequency drop event, the WTG would stall, thus worsening frequency stability, which may result in a double frequency dip, and even frequency instability in extreme cases. Hence, calculating the WTGs rotor speed is necessary, which has not yet been done to the best knowledge of the authors in other papers. Therefore, the following contributions are made in this paper:

- A novel analytical frequency model for power system large-perturbation studies is proposed, which provides the WTG internal response through explicit equations for its kinetic energy and speed.
- Two methods for tuning typical VICs are also proposed based on the proposed WTG nonlinear model; the first approach guaranties the WTG frequency stability for FDs, and the second one additionally maximizes the WTG inertial participation.

The proposed model could be also useful for other power system studies such as economic impact of wind power integration [15]–[17], and utilization of energy storage for system frequency support [18]–[21].

The rest of this paper is organized as follows: Section II briefly discusses existing frequency models of the system and WTGs, as well as a typical VIC. In Section III, the proposed large-perturbation modeling of WTGs is discussed. Two new tuning methods for VICs based on this model are proposed in

M. H. Ravanji and M. Parniani are with the Electrical Engineering Department, Sharif University of Technology, Tehran, Iran (e-mail: ravanji@ee.sharif.edu; parniani@sharif.edu).

C. Cañizares is with the Department of Electrical and Computer Engineering, University of Waterloo, Waterloo, ON, Canada (email: ccanizar@uwaterloo.ca).

Section IV. Simulation results to test, validate, and compare the proposed WTG model and VIC tuning approaches are presented in Sections V and VI. Finally, conclusions are drawn in Section VII.

II. Background Review

In this section, the frequency models of power system and the WTG components are first described. A typical VIC is also presented here.

A. Power System Frequency Model

The fundamental concern in power system frequency stability is the active power balance between generators and loads. Since the generators output power is controlled by governors, the overall power system frequency model can be described by the system swing equation as follows [22]:

$$\Delta P_m(t) - \Delta P_e(t) = 2H_s \frac{d}{dt}\Delta\omega_s(t) + D_s\Delta\omega_s(t) \tag{1}$$

where ΔP_m, ΔP_e, and $\Delta\omega_s$ denote the system overall mechanical and electrical power changes and the system frequency deviations, respectively. In addition, H_s represents the system inertia constant, and D_s is defined as follows:

$$D_s = \frac{\Delta P_L}{\Delta\omega_s} \tag{2}$$

which describes the sensitivity of frequency-dependent loads to system frequency changes. Assuming that the equivalent system governor-turbine transfer function is represented by $G(s)$, ΔP_m can be calculated as follows:

$$\Delta P_m(s) = G(s)\Delta\omega_s(s) \tag{3}$$

Note that ΔP_e is controlled by an AGC, in order to preserve the system frequency at its nominal value, by gradually changing the system generators set points to balance the total load and generation. However, compared to the inertial and primary frequency-control response, the AGC is quite slow, and thus its effect is not considered in this paper, which focuses on primary frequency control. It should be highlighted that the inclusion of AGC improves the system frequency response, and thus the proposed models provide conservative results.

B. WTG Frequency Model

WTGs respond to power system perturbations as per their swing equation, as follows [21]:

$$\frac{P_{m,WT} - P_{e,WT}}{\omega_m} = 2H_{WT}\frac{d}{dt}\omega_m \tag{4}$$

where $P_{m,WT}$, $P_{e,WT}$, H_{WT}, and ω_m denote the WTG mechanical and electrical powers, its intrinsic inertia constant, and its rotor speed, respectively. The WTG mechanical power is a function of the wind speed, WTG rotor speed, and its pitch angle, which is controlled by a pitch angle controller that, due to mechanical restrictions, confines the WTG output power to its nominal value for wind speeds higher than the WTG nominal speed. On the other hand, in order to extract the maximum wind power, the WTG electrical power is controlled through a Maximum Power-Point Track (MPPT) approach, which regulates the WTG rotor speed as well. Accordingly, the WTG electrical power is independent of the system frequency and is not influenced by the FDs, i.e. WTGs do not typically participate in the system frequency ancillary services. However, VICs are being introduced to remedy this situation, given the higher penetration of WTGs in the grid, which requires that WTGs contribute to frequency regulation, as per various current grid codes [6], [23], [24].

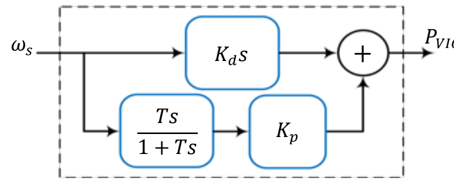

Fig. 1. Block diagram of a common VIC.

C. Existing VIC Model

VICs affect the WTG electrical power reference as follows:

$$P^*_{e,WT} = P_{MPP} - P_{VIC} \tag{5}$$

where P_{MPP}, P_{VIC}, and $P^*_{e,WT}$ denote the MPPT reference power, VIC output signal, and the WTG electrical power reference, respectively. The structure of a typical VIC is illustrated in Fig. 1. Observe that the VIC is made up of two controllers: a derivative controller with gain K_d emulating the inertial response of a conventional generator, and a proportional controller with gain K_p providing temporary droop for the WTG during FDs. Note that the VIC requires the "frequency changes" as its input signal, with some papers providing this by subtracting the system frequency from its reference (e.g. [5]), while others provide this through a washout filter, which removes the dc component of the system frequency (e.g. [25] and [26]). In the former approach, when a large load/generation change occurs in the system, primary frequency regulation balances the generation and the load, stabilizing the frequency at a value that is not its nominal value, requiring some time for the AGC to restore the system frequency to its nominal value; during this period, the VIC has a dc input signal forcing the WTG to provide unnecessary inertial response for the system. On the other hand, in the latter, the washout filter eliminates this unnecessary inertial provision. Furthermore, the washout filter transfer function has a rather small negative real pole while the derivative controller has a large negative real pole, which combined make the VIC casual.

When a frequency drop occurs, the VIC changes the WTG electrical power reference and, given the fast responses of the power electronic components and controllers, the WTG output power increases rapidly. However, the mechanical power does

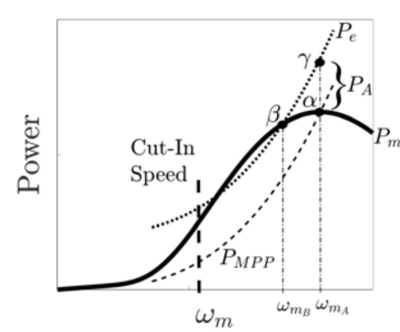

Fig. 2. WTG internal response after a frequency drop in the system.

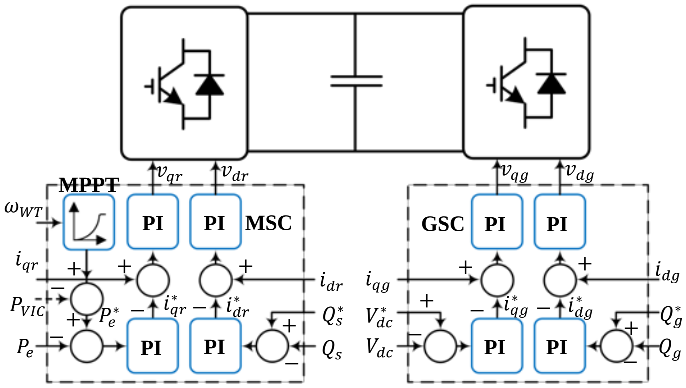

Fig. 3. WTG simplified control scheme.

not change as fast as the electrical power; therefore, according to (4), the negative accelerating power decelerates the WTG. Fig. 2 describes the WTG internal response when a frequency drop occurs, where point α corresponds to the WTG steady-state operating point before the frequency drop, point β represents its steady-state operating point after the frequency drop, and point γ stands for a time snapshot when $P_{VIC} = -P_A$, after the frequency drop; thus, when the frequency changes, the WTG rotor speed decreases and its operating point moves from point α to β, passing through γ.

D. *WTG Internal Control Scheme*

The overall control scheme of existing variable speed WTGs is illustrated in Fig. 3 [27]. Observe that the active power is regulated through a cascade scheme of PI controllers, where the reference is determined using the wind turbine rotor speed via the MPPT function, which may be then modified by an optional VIC output signal. In addition to the WTG active power, the stator and grid-injected reactive powers, and the dc-link capacitor voltage are regulated by the machine-side controller (MSC) and the grid-side controller (GSC).

III. Large-Perturbation Modeling

As mentioned in Section I, an approximated nonlinear model is presented here providing the required equations for evaluating the WTG internal response when an FD occurs in the power system. Thus, in a power system with VIC-equipped WTGs, for low penetration wind power, the overall power system inertia constant H_e and load damping D_e are approximately equal to the corresponding system parameters of an equivalent synchronous generator's H_s and D_s, respectively. On the other hand, for high WTG penetration, one has [28]:

$$H_e = H_s + \frac{PR}{2} K_d \tag{6}$$

$$D_e = D_s + PR\, K_p \tag{7}$$

where PR denotes the WTG penetration ratio.

The system equivalent governor-turbine can be simplified as follows [29]:

$$G(s) = K_G \frac{1 + sT_{G1}}{1 + sT_{G2}} \tag{8}$$

where T_{G1} and T_{G2} represent the time constants of the equivalent governor, and K_G is its gain. Several standard IEEE governor-turbine models are available in the literature [30]; however, as discussed in [29], transfer function (8) can effectively describe any complex governor responses for frequency stability and control studies. Therefore, the frequency can be calculated from the power system frequency model, as follows:

$$\Delta\omega_s(s) = \frac{\Delta U(s) - K_G \frac{1 + sT_{G1}}{1 + sT_{G2}} \Delta\omega_s(s) + \Delta P_{e,WT}}{2H_e s + D_e} \tag{9}$$

where $\Delta U(s)$ denotes the system power variation. In the presence of an FD, the power variation is modeled by a step change $\Delta U(s) = -\frac{\Delta P_L}{s}$, where ΔP_L represents the amount of active load/generation decrease/increase. Major load power changes are mainly compensated by dispatching synchronous generators, with WTGs' output powers not significantly changing, i.e. one can assume that $\Delta P_{e,WT} \ll \Delta P_L$, since WTGs are used here to help synchronous generators with frequency regulation, as WTGs are not capable of compensating for large power changes in the system, because these are not dispatchable. Based on these assumptions, the system frequency can be obtained from (9) as follows:

$$\Delta\omega_s(s) = -\frac{\Delta P_L}{s} \frac{\frac{1}{2H_e T_{G2}} + \frac{s}{2H_e}}{s^2 + \frac{s}{T_{d1}} + \left(\frac{1}{T_{d2}}\right)^2} \tag{10}$$

where:

$$T_{d1} = \frac{2H_e T_{G2}}{2H_e + D_e T_{G2} + K_G T_{G1}} \tag{11}$$

$$T_{d2} = \sqrt{\frac{2H_e T_{G2}}{D_e + K_G}} \tag{12}$$

Using the Inverse Laplace Transform, the time-domain response of the system frequency can be calculated as follows:

$$\Delta\omega_s(t) = -\frac{\Delta P_L}{P_1 P_2}\left(e^{-\frac{t}{2T_{d1}}} sin(\omega_d t - \phi) + P_2\right) \tag{13}$$

where:

$$\omega_d = \frac{\sqrt{4\eta^2 - 1}}{2T_{d1}} \tag{14}$$

$$\phi = cot^{-1}\zeta \tag{15}$$

$$\eta = \frac{T_{d1}}{T_{d2}} \tag{16}$$

$$\zeta = \frac{2\eta \frac{T_{G2}}{T_{d2}} - 1}{\sqrt{4\eta^2 - 1}} \tag{17}$$

$$P_1 = \frac{2H_e T_{G2}}{T_{d2}^2} \tag{18}$$

$$P_2 = \frac{1}{\sqrt{\zeta^2 + 1}} \tag{19}$$

In order to calculate the WTG internal response, the VIC transfer function in Fig. 1 can be used, yielding:

$$\Delta P_{VIC}(s) = \left(K_d s + K_P \frac{Ts}{1+Ts}\right)\Delta\omega_s(s) = \Delta P_{VIC}^{K_d}(s) + \Delta P_{VIC}^{K_p}(s) \tag{20}$$

where:

$$\Delta P_{VIC}^{K_d}(s) = K_d s \Delta\omega_s(s) \tag{21}$$

$$\Delta P_{VIC}^{K_p}(s) = \left(K_p - \frac{K_p}{1+Ts}\right)\Delta\omega_s \tag{22}$$

In the time domain:

$$\Delta P_{VIC}^{K_d}(t) = K_d \frac{d}{dt}\Delta\omega_s(t) \tag{23}$$

$$\Delta P_{VIC}^{K_p}(t) = K_p\left(\Delta\omega_s(t) - \mathcal{L}^{-1}\left\{\frac{1}{1+Ts}\right\} * \Delta\omega_s(t)\right) \tag{24}$$

Thus, using the Inverse Laplace Transform, the following equations can be obtained:

$$\Delta P_{VIC}^{K_d}(t) = \frac{\Delta P_L}{P_1 P_2} K_d \omega_d' e^{-\frac{t}{2T_{d1}}} sin(\omega_d t - \phi_1) \tag{25}$$

$$\Delta P_{VIC}^{K_p}(t) = -\frac{\Delta P_L}{P_1 P_2} K_p \left[\frac{e^{-\frac{t}{2T_{d1}}}}{T''\omega_d''} sin(\omega_d t - \phi_p) + \frac{e^{-\frac{t}{T}}}{T\omega_d''}(T\omega_d'' P_2 - sin\,\phi_1)\right] \tag{26}$$

where:

$$\omega_d' = \sqrt{\omega_d^2 + \left(\frac{1}{2T_{d1}}\right)^2} = \omega_d\sqrt{1+\zeta'^2} \tag{27}$$

$$\omega_d'' = \sqrt{\omega_d^2 + \left(\frac{1}{T} - \frac{1}{2T_{d1}}\right)^2} = \omega_d\sqrt{1+\zeta''^2} \tag{28}$$

$$\zeta' = \frac{-1}{2T_{d1}\omega_d} \tag{29}$$

$$\zeta'' = \zeta' - \frac{1}{T\omega_d} \tag{30}$$

$$\zeta''' = \zeta'' - T\omega_d''\sqrt{1+\zeta''^2} \tag{31}$$

$$T'' = \frac{1}{\sqrt{\omega_d''^2 \frac{\zeta''' + \zeta''}{\zeta''' - \zeta''} + \frac{1}{T^2}}} \tag{32}$$

$$\phi_p = \phi + \phi''' \tag{33}$$

$$\phi_1 = \phi - \phi' \tag{34}$$

Substituting (25) in (20), and employing the Inverse Laplace Transform, the VIC output signal can then be calculated as follows.

$$\Delta P_{VIC}(t) = -\frac{\Delta P_L}{P_1 P_2 P_3}\left[e^{-\frac{t}{2T_{d1}}} sin(\omega_d t - \phi_V) + P_4 e^{-\frac{t}{T}}\right] \tag{35}$$

where:

$$P_3 = \frac{1}{\sqrt{K_d'^2 + K_p'^2 + 2K_d' K_p' \cos\phi_3}} \tag{36}$$

$$P_4 = \frac{K_p\left(P_2 + \frac{sin\,\phi_2}{T\omega_d''}\right)}{\sqrt{K_d'^2 + K_p'^2 + 2K_d' K_p' \cos\phi_3}} \tag{37}$$

$$K_d' = K_d\omega_d' \tag{38}$$

$$K_p' = \frac{K_p}{T''\omega_d''} \tag{39}$$

$$\phi_2 = \phi + cot^{-1}\,\zeta'' \tag{40}$$

$$\phi_3 = cot^{-1}\,\zeta' - cot^{-1}\,\zeta''' \tag{41}$$

$$\phi_V = \phi_p + cot^{-1}\frac{K_p'/K_d' + \cos\phi_3}{sin\,\phi_3} \tag{42}$$

On the other hand, by defining the WTG kinetic energy $E_r = H_{WT}\omega_m^2$, and rearranging the WTG swing equation, the following equation can be obtained:

$$P_{VIC}(t) = \frac{d}{dt}E_r(t) - \left(P_{m,WT}(t) - P_{MPP}(t)\right) \tag{43}$$

It is not possible to solve (43) analytically; however, detailed numerical simulations show that $P_{m,WT}(t) - P_{MPP}(t)$ reflects the delayed behavior of $P_{VIC}(t)$, with this delay being proportional to the WTG intrinsic and emulated inertia. Therefore, based on these empirical observations, the following novel approximations are proposed here:

$$P_{m,WT}(s) - P_{MPP}(s) \cong P_{VIC}(s)\left(-\frac{1}{1+Ks}\right) \tag{44}$$

$$K \cong H_{WT} - P_5\Delta E_{VIC} \tag{45}$$

where P_5 is a fixed parameter that can be obtained from simulations, and ΔE_{VIC} is the released energy by the VIC:

$$\Delta E_{VIC} = \int_{t=0}^{t=\infty} \Delta P_{VIC}(t)\,dt \tag{46}$$

The validity of these approximations is demonstrated with simulation results in Sections V and VI. In order to calculate ΔE_{VIC}, the integral of $\Delta P_{VIC}(t)$ can be derived as follows from (35):

$$\int_{\tau=0}^{\tau=t} \Delta P_{VIC}(\tau)\,d\tau = \frac{\Delta P_L}{P_1 P_2 P_3'}\left[e^{-\frac{t}{2T_{d1}}} sin(\omega_d t - \phi_I) + P_4' e^{-\frac{t}{T}} + sin\,\phi_I + P_4'\right] \tag{47}$$

where $P_3' = P_3\omega_d'$, $P_4' = P_4 T\omega_d'$, and $\phi_I = \phi_V + \cot^{-1}\zeta'$. Then, at $t = \infty$, one has:

$$\Delta E_{VIC} \cong \frac{\Delta P_L}{P_1 P_2 P_3'}(\sin\phi_I + P_4') \tag{48}$$

Thus, substituting (48) in (45), it follows that:

$$K \cong H_{WT} - P_5 \frac{\Delta P_L}{P_1 P_2 P_3'}(\sin\phi_I + P_4') \tag{49}$$

and by substituting (49) in (44), the WTG swing equation can be simplified to:

$$P_{VIC}(s)\left(-\frac{1}{1+Ks}+1\right) \cong sE_r(s) \tag{50}$$

Substituting (35) in (50), and using the Inverse Laplace Transform, the WTG energy can be obtained as follows:

$$\Delta E_r(t) = \frac{\Delta P_L}{P_1 P_2 P_{3K}}\Big[e^{-\frac{t}{2T_{d1}}}\sin(\omega_d t - \phi_E) + P_{4K}e^{-\frac{t}{T}} - P_{5K}e^{-\frac{t}{K}}\Big] \tag{51}$$

where $P_{3K} = P_3\omega_{dK}$, $P_{4K} = P_4\frac{TK}{K-T}\omega_{dK}$, $P_{5K} = P_{4K} - \sin\phi_E$, $\phi_E = \phi_V + \cot^{-1}\zeta_K$, and:

$$\zeta_K = \zeta' + \frac{1}{K\omega_d} \tag{52}$$

$$\omega_{dK} = \omega_d\sqrt{1+\zeta_K^2} \tag{53}$$

Therefore, by rearranging the WTG kinetic energy equation, the internal response of the WTG can be obtained from:

$$\omega_m(t) = \sqrt{\frac{E_r(t)}{H_{WT}}} = \sqrt{\omega_{m0}^2 + \frac{\Delta E_r(t)}{H_{WT}}} \tag{54}$$

where ω_{m0} denotes the WTG rotor speed at the instance of the FD occurrence.

Employing the proposed model, the system frequency (13), VIC output signal (35), WTG kinetic energy (51), and its rotor speed (54) can be obtained sequentially. It should be mentioned that in detailed turbine-governors and WTG models, there are several nonlinearities and saturations associated with practical component limitations. These limitations have not been considered here; however, as shown in Sections V and VI, including these limitations do not significantly affect the results, thus showing that the proposed model is sufficiently accurate.

IV. VIC TUNING

As previously discussed, increasing WTG penetration requires the participation of these generators in system frequency control; however, WTG energy release to the system may destabilize these generators, because there is a minimum limit for the WTG rotor speed ω_m^{stall}, which if reached, stalls the WTGs. This instability may occur when the wind speed is low and is near the WTG cut-in speed, since in this condition the MPPT regulates the WTG rotor speed near the ω_m^{stall}, with the WTG energy released possibly stalling these generators. In order to avoid this, two new and distinct methods for tuning the VICs are proposed, which are derived from the proposed large-perturbation model. For this purpose, the VIC gains are initially obtained by conventional methods described in [7], [12], [15], and [23], which do not change with wind speed variations; then, these gains are modified using the proposed techniques described next. In the first method, the typical gains are scaled for the worst-case scenario, and in the second method, a nearly optimum gain scaling factor is obtained for a specific wind speed.

A. Worst-Case Scenario (WCS) Tuning

In this method, it is assumed that a maximum conceivable load/generation (MCLG) change is specified, and that the VIC gains are tuned to avoid WTG instability for this worst-case scenario, i.e. the conventional VIC gains are scaled for the WCS. For the sake of comparison with a typical VIC gain, the following tuning scaling factor is defined and used here:

$$VR = \frac{Tuned\ VIC\ Gain}{Typical\ VIC\ Gain} \tag{55}$$

In the WCS method, VR is calculated for the worst-case scenario, i.e. the VIC gains are calculated for the MCLG change, at the minimum expected WTG rotor speed $\omega_m^{min} = \omega_m^{stall}$. If $VR \geq 1$, the WTG equipped with a typical VIC is internally stable; on the other hand, if $VR < 1$, the WCS method attenuates the VIC gains to guarantee the WTG internal stability, providing the expected inertial response for the system and thus injecting the required energy for the system to recover, even for severe frequency drops. However, with this method, the VIC gain is reduced for all wind speeds; thus, even at higher wind speeds when the turbine instability is not an issue, the VIC effect is also attenuated, which reduces the effectiveness of the WTG emulated inertial response. To address this issue, an optimal VIC tuning method is proposed next.

B. Optimal Tuning

The main objective of employing VICs for WTGs is to provide inertial response for the system to improve its frequency response. However, there are several limitations to consider, such as WTG stability at lower wind speeds as previously discussed. The WTG maximum output power $P_{e,WT}^{nom}$ and its maximum allowable output power rate of change $\rho_{e,WT}$ are other limitations that must be considered when tuning VICs. Thus, in order to optimize the VIC gain, the following optimization problem is proposed here:

$$\min \quad \omega_m^{min} \tag{56}$$

$$\text{s.t.} \quad \omega_m \geq \omega_m^{stall} \tag{57}$$

$$\left|\frac{d}{dt}P_{e,WT}\right| \leq \rho_{e,WT} \tag{58}$$

$$P_{e,WT} \leq P_{e,WT}^{nom} \tag{59}$$

where constraint (57) stands for the WTG stability at lower wind speed, (58) represents the WTG maximum allowable output power rate of change, and (59) corresponds to the WTG maximum output power. This optimization problem is nonlinear and should be solved for various wind speeds, which is accomplished here by determining its feasibility region. Thus, first constraints (58) and (59) are ignored and the inequality constraint (57) is considered as an equality constraint. Then, for various wind speeds in their normal range, with a small step of 0.1 m/s, VR in (55) is calculated from equations (6)-(54) for each wind speed assuming $\omega_m = \omega_m^{stall}$ from (57), thus generating a set of VR values that are interpolated using a quadratic polynomial; this procedure yields the red line for constraint (57) depicted in Fig. 4. A similar procedure is used for the two other constraints (58) and (59), i.e. for (58), constraints (57) and (59) are ignored and (58) is considered as an equality constraint, and for (59), constraints (57) and (58) are ignored and (59) is considered as an equality constraint; these yield the blue line for (58) and the black line for (59) in Fig. 4. This procedure gives the feasible space for the optimization problem (56)-(59) depicted in Fig. 4 for a specific MCLG value. A parabolic function can then be defined for VR by interpolating points A, B, and C in Fig. 4, which approximates the feasible space boundary of the optimization problem. Thus, for a wind speed v_W, the near-optimal VIC gains can be obtained by using this quadratic function to get the gain scaling factor VR for a given MCLG. Note that this VR value does not attenuate the WTG inertial response at high wind speeds, as opposed to the previously proposed WCS method, while guaranteeing the WTG internal stability and providing the expected inertial response for the system, even for severe frequency drops.

V. Two-Area Four-Machine Test System Results

In this section, in order to examine the performance of the proposed model and the proposed VIC tuning methods, a modified version of the IEEE two-area four-machine test system illustrated in Fig. 5 is used, consisting of a 300-MW DFIG-based wind farm and three 900 MW synchronous generators [31]. The aggregated wind farm represents 200 1.5 MW GE WTGs, for wind speeds in the range of 6 to 12 m/s assuming MPPT control, which is modeled using the phasor representation proposed in [32]. The default value of the wind speed is 11 m/s at which the wind farm generates 167.7 MW at 1.01 pu bus voltage. The system parameters can be found in the Appendix. It should be highlighted that the proposed models are valid for DFIG as well as full converter WTGs, and thus similar results would be expected for the latter.

The synchronous generators are modeled as single-mass tandem-compound generators equipped with the IEEE Type-I turbine governors and excitation systems [30]; as previously mentioned, the AGC is not included here. At the default operating point, SG2, SG3, and SG4 generate 489.9 MW, 698.7 MW, and 698.7 MW at set-point voltages 1.03 pu, 1.03 pu, and 1.01 pu, respectively. As the wind speed changes, the WTG MW output changes (as a cubic function), with the SG2 output being re-dispatched to compensate for these changes, thus assuming this generator to be the system slack bus, so that the system frequency is kept within permissible bounds.

The implemented VIC for the aggregated wind farm is illustrated in Fig. 1. The most appropriate input signal for this VIC is the voltage frequency at Bus 1; however, since this signal is not available in phasor-based simulations, the per-unit value of the SG2 rotor speed, which is the closest generator, is used as the system frequency input to the VIC. Furthermore, the VIC output signal is assumed to be in per unit with respect to the WTG base.

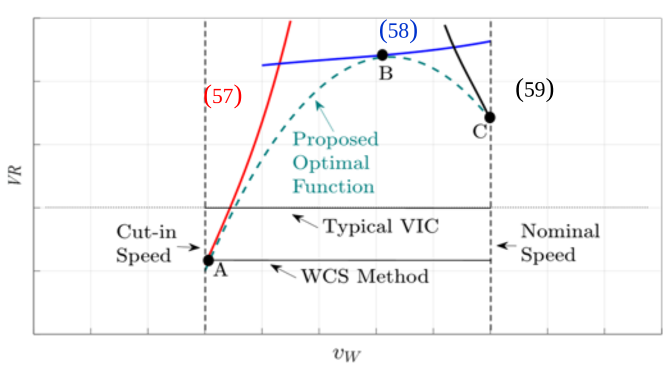

Fig. 4. VR solution space and limits.

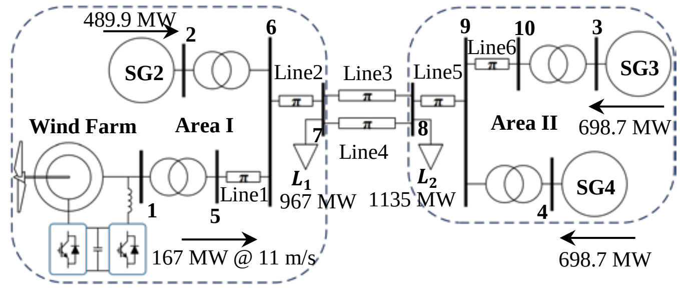

Fig. 5. Modified IEEE two-area four-machine test system [2].

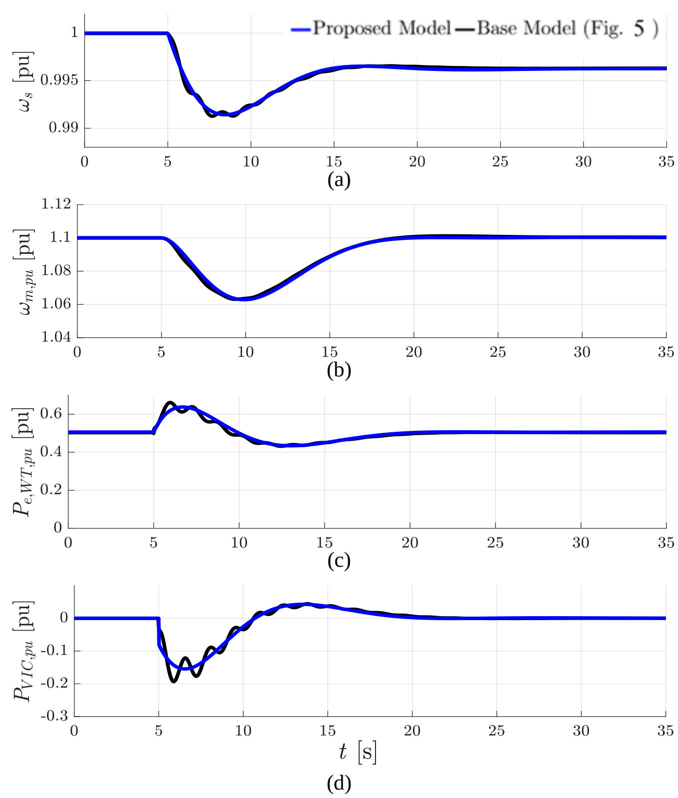

Fig. 6. Simulation results for $v_W = 11$ m/s and 200 MW load change at Bus 8 at $t = 5$ s: (a) system frequency, (b) WTG rotor speed, (c) WTG output electrical power, and (d) VIC output signal.

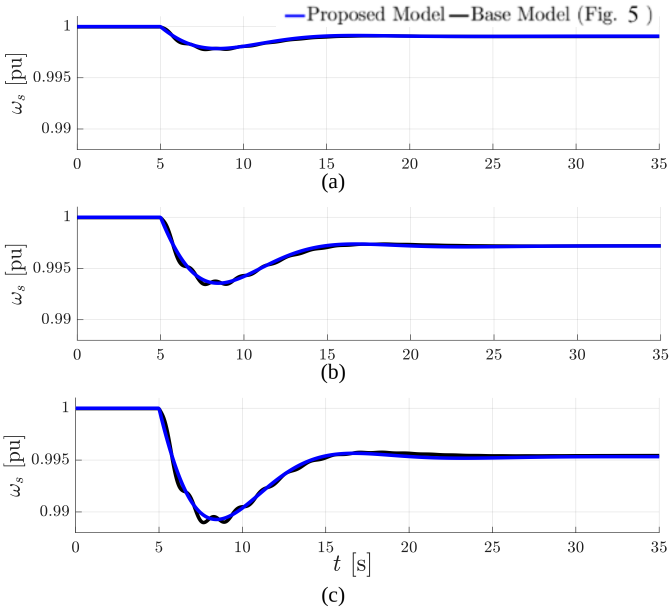

Fig. 7. System frequencies for $v_W = 11$ m/s and Bus 8 load changes at $t = 5$ s: (a) 50 MW, (b) 150 MW, and (c) 250 MW.

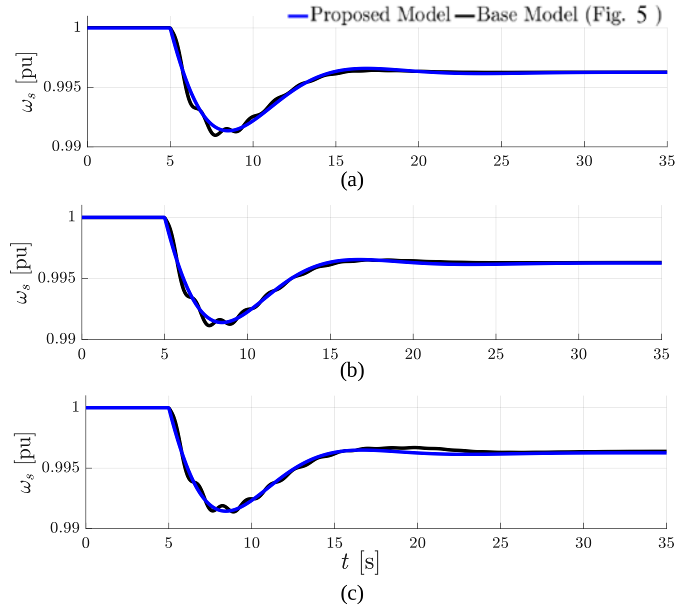

Fig. 8. System frequencies for a 200 MW load change at Bus 8 $t = 5$ s, and wind speeds: (a) 8 m/s, (b) 10 m/s, and (c) 12 m/s.

The synchronous inertia constant of the system H_s can be calculated by adding the weighted inertia constants of each synchronous generator, where the weights are proportional to their rated power. On the other hand, D_s, K_G, $T_{G1,}$ and T_{G2} were obtained using the curve-fitting toolbox in MATLAB/Simulink [33], which was used for all simulations, to match the simulation results of the base model with the proposed model response for several load changes. Numerical values of the all system parameters used in the closed-from expressions in (6)-(54) can be found in the Appendix.

A. Model Validation

In order to verify the validity of the obtained equations and the corresponding proposed model in Section III, at $t = 5$ s a 200 MW impedance load is added at Bus 8. The obtained results are depicted in Fig. 6 for both detailed and proposed models of the WTG. Observe that the proposed equations yield accurate values for the system frequency, the VIC output signal, and the WTG rotor speed and its output power. Furthermore, as mentioned earlier, in order to investigate the effect of the systems nonlinearities, the simulations are repeated for several load changes and wind speeds, as depicted in Fig. 7 and Fig. 8, showing only the system frequency results. Note that even for large load changes and high wind speeds, the frequency response obtained from the proposed model is accurate.

B. VIC Tuning

As previously discussed, inertial contributions from WTGs at low wind speed conditions can destabilize these generators. In order to study this issue and also to verify the performance of the proposed VIC tuning methods, the wind speed is assumed to be 7 m/s in the test system, with the following load increases at Bus 8 at $t = 5$ s: 100 MW, 200 MW, and 300 MW. The simulation results are presented in Fig. 9, where for the 300 MW load increase, the WTG rotor speed is less than ω_m^{stall}, thus losing WTG generation and destabilizing the system. To avoid this problem, the two VIC tuning methods proposed here are applied.

First, the VIC gains are tuned using the WCS method. Accordingly, assuming that the MCLG change is 300 MW for this test system, solving (54) for $\omega_m^{min} = \omega_m^{stall}$ yields:

$$VR = 0.55 \tag{60}$$

Thus, the VIC gains should be attenuated by 0.55. For the second tuning approach, the VIC gains were obtained based on the feasible solution space of (56). Accordingly, assuming that the MCLG change is 300 MW and $\rho_{e,WT} = 0.5$ pu/s, the following parabolic equation can be obtained for VR:

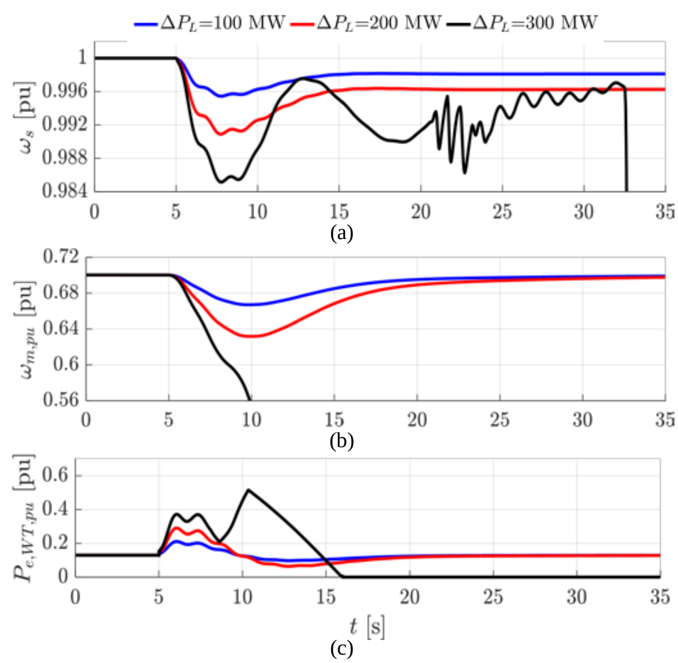

Fig. 9. Simulation results for $v_W = 7$ m/s and 100, 200, and 300 MW load increases at Bus 8 at $t = 5$ s: (a) system frequency, (b) WTG rotor speed, and (c) WTG power output.

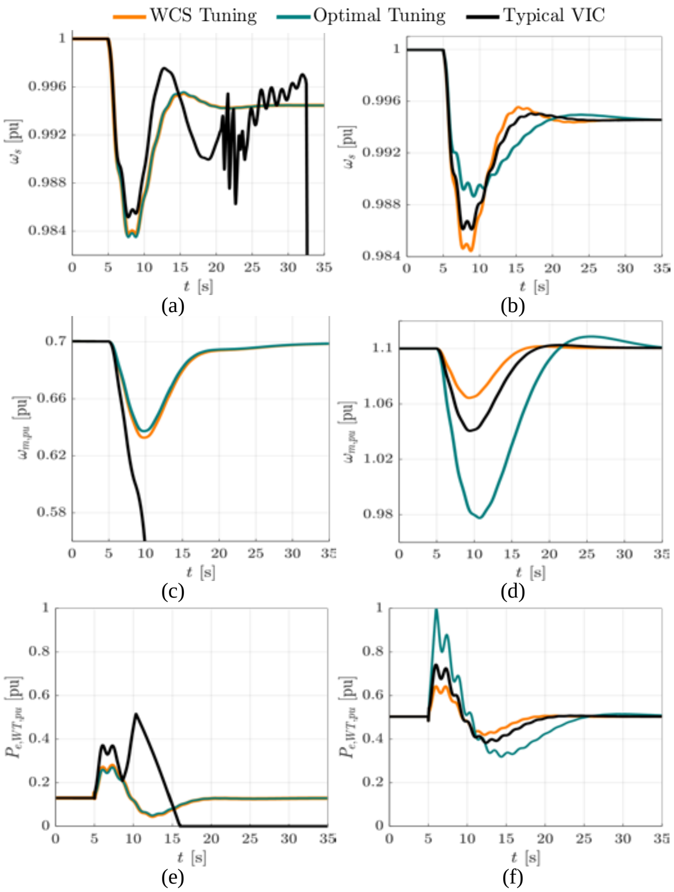

Fig. 10. Simulation results for 300 MW load increase at Bus 8 at $t = 5$ s: (a) system frequency for $v_W = 7$ m/s, (b) system frequency for $v_W = 11$ m/s, (c) WTG rotor speed for $v_W = 7$ m/s, (d) WTG rotor speed for $v_W = 11$ m/s, (e) WTG output power for $v_W = 7$ m/s, and (f) WTG output power for $v_W = 11$ m/s.

$$VR = -23\left(\frac{v_W}{v_{W,b}}\right)^2 + 40\left(\frac{v_W}{v_{W,b}}\right) - 15 \tag{61}$$

The simulation results for a 300 MW load increase at Bus 8, for wind speeds 7 m/s and 11 m/s, with both tuning methods are depicted in Fig. 10. Observe that the WTG rotor speed never reaches its ω_m^{stall} limit, and thus the power system instability problem at lower wind speeds is resolved. Note also that in scenarios with higher wind speeds, the WCS method decreases the WTG inertial participation, while the optimization approach provides more inertial response from the WTG, improving the system frequency response, as expected.

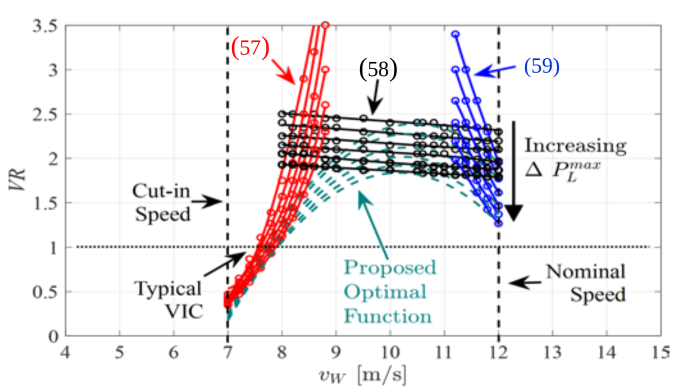

Fig. 11. Feasibility space for VR in (56), and WTG limits for various MCLG values.

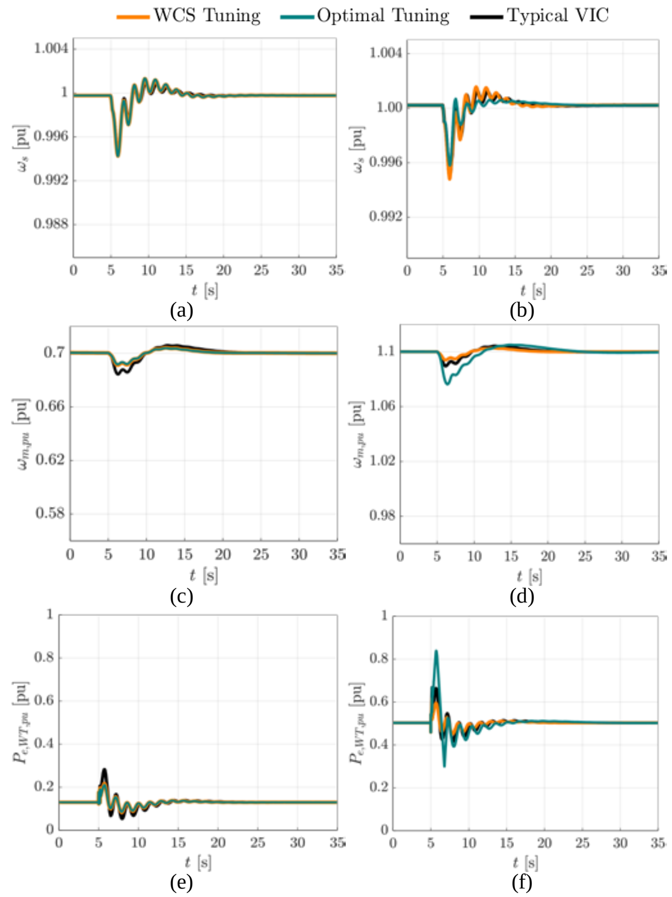

Fig. 12. Simulation results for a three-phase fault at Bus 8 at $t = 5$ s, cleared 10 cycles later: (a) system frequency for $v_W = 7$ m/s, (b) system frequency for $v_W = 11$ m/s, (c) WTG rotor speed for $v_W = 7$ m/s, (d) WTG rotor speed for $v_W = 11$ m/s, (e) WTG output power for $v_W = 7$ m/s, and (f) WTG output power for $v_W = 11$ m/s.

Finally, by solving optimization problem (56)-(59) for various MCLG values, Fig. 11 is obtained, illustrating the solution of the optimization problem as MCLG changes, thus showing the effect of MCLG on the optimal VR. Note that as MCLG increases, the optimum values for VR decrease, which means that for more severe FDs, the WTG inertial participation decreases as well.

C. Three-Phase Fault

In order to investigate the response to severe disturbances of the system equipped with a tuned VIC, the simulation results for a three-phase fault at Bus 8 at $t = 5$ s, cleared 10 cycles later, are depicted in Fig. 12 for wind speeds 7 m/s and 11 m/s. Observe that the system stability is preserved, due to the fact that the fault is cleared in less than a second and the VIC is properly tuned. As in previous simulations, the optimally tuned VIC presents the best performance.

VI. New England 10-Machine 39-Bus System Results

In this section, in order to examine the performance of the proposed model and VIC tuning methods in a more realistic system, the IEEE 10-machine, 39-bus New England test system in [13] has been modified by adding a wind farm at Bus B22, consisting of 500 1.5 MW GE WTGs similar to the two-area

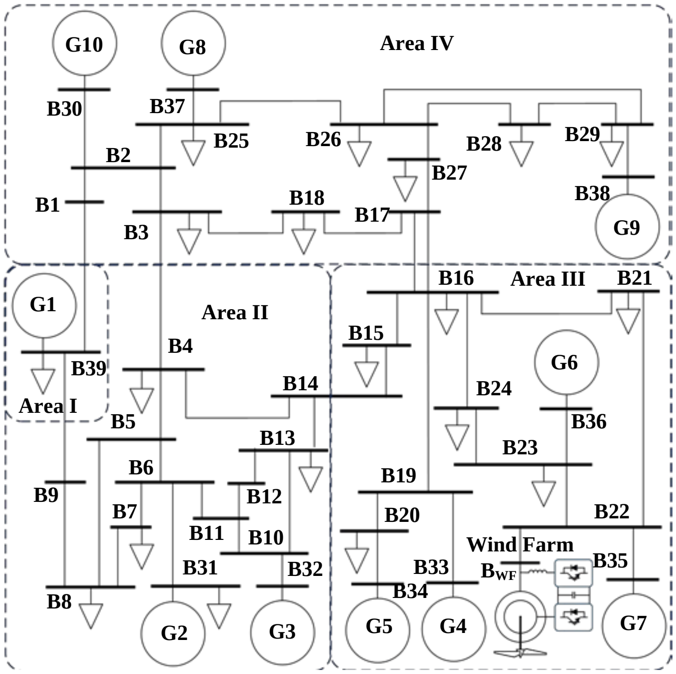

Fig. 13. Modified IEEE 10-machine 39-bus New England test system.

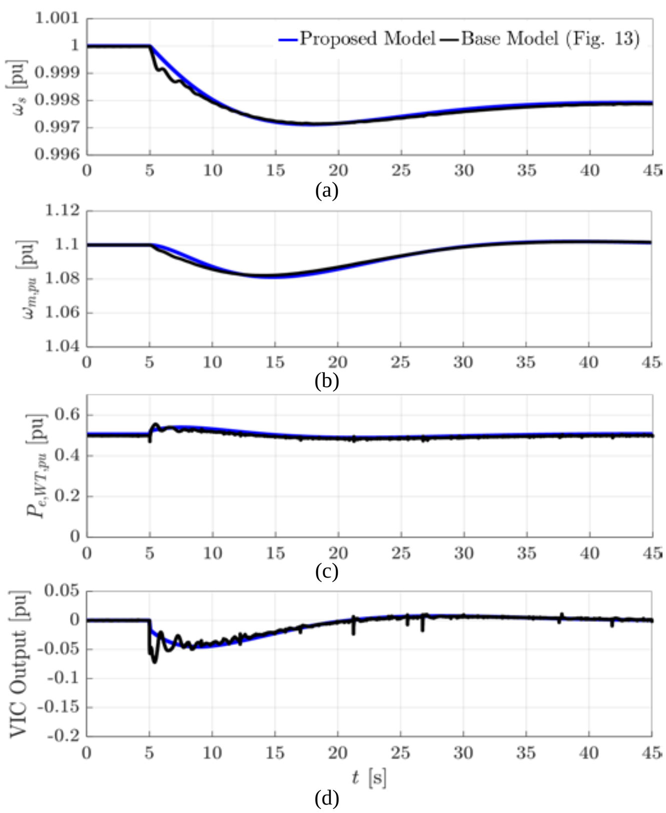

Fig. 14. Results for $v_W = 11$ m/s and 500 MW impedance load change at Bus B11 at $t = 5$ s for the test system in Fig. 13: (a) system frequency, (b) WTG rotor speed, (c) WTG output electrical power, and (d) VIC output signal.

test system, as illustrated in Fig. 13. The AGC is not included either in this case, and the per unit value of the G7 rotor speed, which is the closest generator, is used as the system frequency input to the VIC, since the voltage frequency at Bus B22 is not available in phasor-based simulations. The values of all system parameters used in the closed-from expressions (6)-(54) can be found in the Appendix.

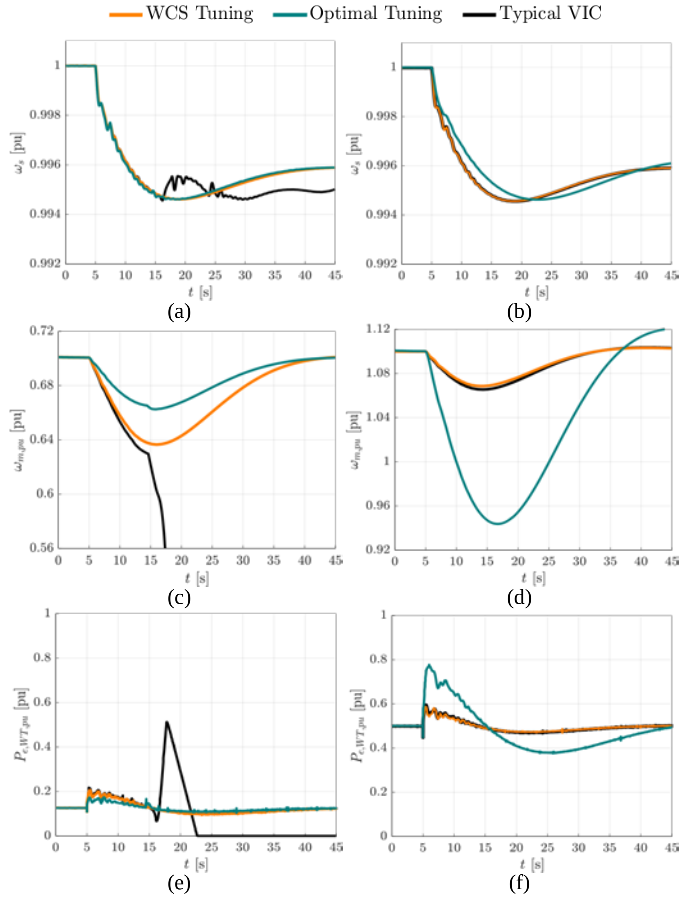

Fig. 15. Simulation results for a 1000 MW impedance load connection at Bus B11 at $t = 5$ s for the test system in Fig. 13: (a) system frequency for $v_W = 7$ m/s, (b) system frequency for $v_W = 11$ m/s, (c) WTG rotor speed for $v_W = 7$ m/s, (d) WTG rotor speed for $v_W = 11$ m/s, (e) WTG output power for $v_W = 7$ m/s, and (f) WTG output power for $v_W = 11$ m/s.

In order to test and compare the model proposed in Section III, a 500 MW impedance load is added to Bus B11 at $t = 5$ s. The obtained results are depicted in Fig. 14 for both detailed and proposed WTG models. Observe that the proposed equations yield accurate values for the system frequency, the VIC output signal, and the WTG rotor speed and output power.

To verify the performance of the proposed VIC tuning methods, the simulation results for a 1000 MW impedance load connection at Bus B11, for wind speeds 7 m/s and 11 m/s, are depicted in Fig. 15 for all tuned VICs. In this case, assuming an MCLG change of 1104 MW (the largest load in the system at Bus B39), and $\rho_{e,WT} = 0.5$ pu/s, the WCS method yields a $VR = 0.9$, whereas the VR value for the optimal tuning method is obtained from the following parabolic function approximating the feasible region of the optimization problem (56)-(59):

$$VR = -52\left(\frac{v_W}{v_{W,b}}\right)^2 + 89.5\left(\frac{v_W}{v_{W,b}}\right) - 34 \qquad (62)$$

Observe that for both tuning methods, the power system instability problem at lower wind speeds detected for the typical VIC is resolved. Note also that at higher wind speeds, the optimization approach provides more inertial response from the WTG, as expected.

VII. Conclusion

In order to investigate the behavior of WTGs equipped with VICs to respond to power system frequency events, a nonlinear WTG model was proposed in this paper, which represents the WTG internal response to large perturbations in the system. This model was then employed to tune VICs to provide optimal inertial response and to avoid WTG instability at lower wind speeds. The adequate performance of the developed model and the proposed tuning methods were verified through several simulations on a test system. The obtained results demonstrate that the presented WTG model and VIC tuning techniques would allow designing better frequency regulation controls for variable speed WTGs, as required in grids with high penetration of wind power sources.

It should be mentioned that the proposed models and techniques may be used for systems with multiple wind farms by simply applying them to each farm at a time, using an aggregated model of the power system that includes the other wind farms. This way each farm would provide proper inertial response while accounting for the effect of the other wind farms, and thus not requiring of centralize coordination of the various VICs.

Appendix

The simulated equivalent WTG and the two-area four-machine system parameters are provided in Tables I and II; the rest of the systems parameters can be found in [13] and [31]. The numerical values of the aggregated system parameters in (6)-(54) used in Sections V and VI are presented in Tables III and IV, respectively.

Table I
Simulated WTG Parameters

Symbol	Name	Value
R_s	Stator resistance	0.00706 pu
R'_r	Rotor resistance	0.005 pu
$L_{l,s}$	Stator leakage inductance	0.171 pu
$L'_{l,r}$	Rotor leakage inductance	0.156 pu
L_m	Magnetizing inductance	2.9 pu
Z	Grid-side coupling inductor	0.0015+j0.15 pu
V_n	Grid-side line voltage	575 V
V_{dc}	DC bus voltage	1200 V
$v_{W,b}$	Base wind speed	12 m/s
H_{WT}	DFIG inertia time constant	5.04 s

Table II
Simulated Generators Parameters in Section V

Symbol	Name	Value
f_s	System nominal frequency	60 Hz
V_{nom}	SG2, SG3, and SG4 rated voltage	20 kV
H_{G2}	SG2 inertia constant	6.5 s
H_{G3}	SG3 inertia constant	6.175 s
H_{G4}	SG4 inertia constant	6.175 s
P_{L1}	Bus 7 active load	967 MW
P_{L2}	Bus 8 active load	995 MW

Table III
Model Parameters in Section V

Symbol	Value	Unit
PR	9.01	%
T_{G1}	1.574	s
T_{G2}	10.075	s
K_G	15.602	pu
D_s	0.080	pu
H_s	6.283	pu
K_d	5	pu
K_p	8	pu
T	3	s
T_{d1}	1.729	s
T_{d2}	2.659	s
η	0.6501	-
ω_d	0.2405	pu
ω'_d	0.3761	pu
ω''_d	0.2444	pu
ζ	4.726	-
ζ'	1.204	-
ζ''	0.1834	-
ζ'''	0.7453	-
ϕ	11.95	deg
P_1	19.835	-
P_2	0.2070	-
P_3	0.0261	pu
P_4	-0.7236	-
P_5	1	pu
T''	2.6589	s
K'_d	5.641	pu
K'_p	9.026	pu
P'_3	0.0098	pu
P'_4	-0.8165	-

Table IV
Model Parameters in Section VI

Symbol	Value	Unit
PR	6.08	%
T_{G1}	2.900	s
T_{G2}	10.52	s
K_G	19.803	pu
D_s	0.080	pu
H_s	7.827	pu
K_d	7	pu
K_p	9	pu
T	3	s
T_{d1}	5.358	s
T_{d2}	6.690	s
η	0.8008	-
ω_d	0.1168	pu
ω'_d	0.1495	pu
ω''_d	0.2669	pu
ζ	1.2137	-
ζ'	0.7993	-
ζ''	2.0557	-
ζ'''	1.8304	-
ϕ	39.49	deg
P_1	23.503	-
P_2	1.573	-
P_3	0.0545	pu
P_4	-1.0908	-
P_5	1	pu
T''	6.690	s
K'_d	4.6502	pu
K'_p	22.401	pu
P'_3	0.0081	pu
P'_4	-0.4891	-

References

[1] P. Kundur *et al.*, "Definition and classification of power system stability IEEE/CIGRE joint task force on stability terms and definitions," *IEEE Trans. Power Syst.*, vol. 19, no. 3, pp. 1387–1401, Aug. 2004.

[2] J. Ma, Y. Qiu, Y. Li, W. Zhang, Z. Song, and J. Thorp, “Research on the impact of DFIG virtual inertia control on power system small-signal stability considering the phase-locked loop,” *IEEE Trans. Power Syst.*, vol. 32, no. 3, pp. 2094–2105, May 2017.

[3] S. Ghosh and N. Senroy, “Electromechanical dynamics of controlled variable-speed wind turbines,” *IEEE Syst. J.*, vol. 9, no. 2, pp. 639–646, Jun. 2015.

[4] M. Hwang, E. Muljadi, G. Jang, and Y. C. Kang, “Disturbance-adaptive short-term frequency support of a DFIG associated with the variable gain based on the ROCOF and rotor speed,” *IEEE Trans. Power Syst.*, vol. 32, no. 3, pp. 1873–1881, 2016.

[5] J. Morren, S. W. H. de Haan, W. L. Kling, and J. A. Ferreira, “Wind turbines emulating inertia and supporting primary frequency control,” *IEEE Trans. Power Syst.*, vol. 21, no. 1, pp. 433–434, Feb. 2006.

[6] W. Gao, Z. Wu, J. Wang, and S. Gu, “A review of inertia and frequency control technologies for variable speed wind turbines,” in *25th Chinese Control and Decision Conference (CCDC)*, 2013, pp. 2527–2533.

[7] Z. S. Zhang, Y. Z. Sun, J. Lin, and G. J. Li, “Coordinated frequency regulation by doubly fed induction generator-based wind power plants,” *IET Renew. Power Gener.*, vol. 6, no. 1, pp. 38–47, Jan. 2012.

[8] J. Lee, G. Jang, E. Muljadi, F. Blaabjerg, Z. Chen, and Y. Cheol Kang, “Stable short-term frequency support using adaptive gains for a DFIG-based wind power plant,” *IEEE Trans. Energy Convers.*, vol. 31, no. 3, pp. 1068–1079, Sep. 2016.

[9] G. Ramtharan, J. B. Ekanayake, and N. Jenkins, “Frequency support from doubly fed induction generator wind turbines,” *IET Renew. Power Gener.*, vol. 1, no. 1, pp. 3–9, Mar. 2007.

[10] L. Holdsworth, J. B. Ekanayake, and N. Jenkins, “Power system frequency response from fixed speed and doubly fed induction generator-based wind turbines,” *Wind Energy*, vol. 7, no. 1, pp. 21–35, 2004.

[11] S. Ghosh, S. Kamalasadan, N. Senroy, and J. Enslin, “Doubly fed induction generator (DFIG)-based wind farm control framework for primary frequency and inertial response application,” *IEEE Trans. Power Syst.*, vol. 31, no. 3, pp. 1861–1871, May 2016.

[12] Y. Fu, Y. Wang, and X. Zhang, “Integrated wind turbine controller with virtual inertia and primary frequency responses for grid dynamic frequency support,” *IET Renew. Power Gener.*, vol. 11, no. 8, pp. 1129–1137, 2017.

[13] J. Ma, Z. Song, Y. Zhang, Y. Zhao, and J. S. Thorp, “Robust stochastic stability analysis method of DFIG integration on power system considering virtual inertia control,” *IEEE Trans. Power Syst.*, vol. 32, no. 5, pp. 4069–4079, Sep. 2017.

[14] K. V. Vidyanandan and N. Senroy, “Primary frequency regulation by deloaded wind turbines using variable droop,” *IEEE Trans. Power Syst.*, vol. 28, no. 2, pp. 837–846, May 2013.

[15] N. Farrokhseresht, H. Chávez, and M. R. Hesamzadeh, “Economic impact of wind integration on Primary Frequency Response,” in *IEEE Eindhoven PowerTech*, 2015, pp. 1–6.

[16] X. Zhao, Z. Yan, Y. Xue, and X. P. Zhang, “Wind power smoothing by controlling the inertial energy of turbines with optimized energy yield,” *IEEE Access*, vol. 5, pp. 23374–23382, 2017.

[17] F. Teng and G. Strbac, “Assessment of the role and value of frequency response support from wind plants,” *IEEE Trans. Sustain. Energy*, vol. 7, no. 2, pp. 586–595, Apr. 2016.

[18] S. Pulendran and J. E. Tate, “Energy storage system control for prevention of transient under-frequency load shedding,” *IEEE Trans. Smart Grid*, vol. 8, no. 2, pp. 927–936, Mar. 2017.

[19] J. Liu, J. Wen, W. Yao, and Y. Long, “Solution to short-term frequency response of wind farms by using energy storage systems,” *IET Renew. Power Gener.*, vol. 10, no. 5, pp. 669–678, 2016.

[20] L. Miao, J. Wen, H. Xie, C. Yue, and W. J. Lee, “Coordinated control strategy of wind turbine generator and energy storage equipment for frequency support,” *IEEE Trans. Ind. Appl.*, vol. 51, no. 4, pp. 2732–2742, Aug. 2015.

[21] M. F. M. Arani and E. F. El-Saadany, “Implementing virtual inertia in DFIG-based wind power generation,” *IEEE Trans. Power Syst.*, vol. 28, no. 2, pp. 1373–1384, May 2013.

[22] A. J. Wood, B. F. Wollenberg, and G. B. Sheblé, *Power Generation, Operation, and Control*. Wiley, 2013.

[23] T. Ackermann *et al.*, “European balancing act,” *IEEE Power Energy Mag.*, vol. 5, no. 6, pp. 90–103, Dec. 2007.

[24] H. Jadhav and R. Roy, “A comprehensive review on the grid integration of doubly fed induction generator,” *Int. J. Electr. Power Energy Syst.*, vol. 49, pp. 8–18, 2013.

[25] J. Ying, X. Yuan, J. Hu, and W. He, “Impact of inertia control of DFIG-based WT on electromechanical oscillation damping of SG,” *IEEE Trans. Power Syst.*, vol. 33, no. 3, pp. 3450–3459, May 2018.

[26] Y. Wang, J. Meng, X. Zhang, and L. Xu, “Control of PMSG-based wind turbines for system inertial response and power oscillation damping,” *IEEE Trans. Sustain. Energy*, vol. 6, no. 2, pp. 565–574, Apr. 2015.

[27] M. H. Ravanji and M. Parniani, “Modified virtual inertial controller for prudential participation of DFIG-based wind turbines in power system frequency regulation,” *IET Renew. Power Gener.*, Sep. 2018.

[28] H. Ye, W. Pei, and Z. Qi, “Analytical modeling of inertial and droop responses from a wind farm for short-term frequency regulation in power systems,” *IEEE Trans. Power Syst.*, vol. 31, no. 5, pp. 3414–3423, Sep. 2016.

[29] P. M. Anderson and M. Mirheydar, “A low-order system frequency response model,” *IEEE Trans. Power Syst.*, vol. 5, no. 3, pp. 720–729, Aug. 1990.

[30] SIEMENS, “Dynamic models package Standard-1 GMB dynamic models for PSS® software product suite revision 1.7,” 2012.

[31] P. Kundur, N. J. Balu, and M. G. Lauby, *Power System Stability and Control*, vol. 7. McGraw-hill New York, 1994.

[32] K. Clark, N. W. Miller, and J. J. Sanchez-Gasca, “Modeling of GE wind turbine-generators for grid studies (V4.5),” *GE Energy, 4,* Apr. 2010.

[33] Mathworks. *MATLAB Documentation. (2015)*, [Online]. Available: http://www.mathworks.com/help/matlab.

Mohammad H. Ravanji received the B.Sc. and M.Sc. degrees in electrical engineering from Sharif University of Technology (SUT), Tehran, Iran, in 2012 and 2014, respectively, where he is currently pursuing the Ph.D. degree. His current research interests include renewable energy systems.

Claudio A. Cañizares (S'85, M'91, SM'00, F'07) is a Full Professor and the Hydro One Endowed Chair at the Electrical and Computer Engineering Department of the University of Waterloo. He received the Electrical Engineer degree from the EPN in Quito-Ecuador in 1984, and his MSc (1988) and PhD (1991) degrees in Electrical Engineering are from the University of Wisconsin-Madison. His research activities focus on the study of stability, modeling, simulation, control, optimization, and computational issues in large and small girds and energy systems in the context of competitive energy markets and smart grids. He is an IEEE Fellow, as well as a Fellow of the Royal Society of Canada, where he is currently the Director of the Applied Science and Engineering Division of the Academy of Science, and a Fellow of the Canadian Academy of Engineering. He is also the recipient of the 2017 IEEE PES Outstanding Power Engineering Educator Award, the 2016 IEEE Canada Electric Power Medal, and of various IEEE PES Technical Council and Committee awards and recognitions, holding leadership positions in several IEEE-PES Technical Committees, Working Groups and Task Forces.

Mostafa Parniani (M’96, SM’05) is a professor of Electrical Engineering at Sharif University of Technology (SUT), Tehran, Iran. He received his B.Sc. degree from Amirkabir University of Technology, Iran, in 1987, and the M.Sc. degree from SUT in 1990, both in Electrical Power Engineering. During 1988-90 he worked for Ghods-Niroo Consulting Engineers Co. and for Electric Power Research Center (EPRC) in Tehran. Then, he obtained the Ph.D. degree in Electrical Engineering from the University of Toronto, Canada, in 1995. He was a visiting scholar at Rensselaer Polytechnic Institute, USA, during 2005-2006. He has been a member of several national committees and councils in his field. His research interests include power system dynamics and control, applications of power electronics in power systems and renewable energies.